SCIENCE CHINA Materials ARTICLES

mater.scichina.com link.springer.com

Published online 25 October 2019 | https://doi.org/10.1007/s40843-019-1187-6
Sci China Mater 2020, 63(3): 375–382

Synthesis of $PdH_{0.43}$ nanocrystals with different surface structures and their catalytic activities towards formic acid electro-oxidation

Chenyang Zhan[1], Huiqi Li[1], Xuemin Li[1], Yaqi Jiang[1*] and Zhaoxiong Xie[1,2*]

ABSTRACT **The synthesis of nanocrystals (NCs) with defined morphology and surface structure provides an effective way to investigate the structure-activity relationship of nanocatalytsts, and it will facilitate the design of nanocatalysts with excellent catalytic performance. In this paper, we developed a facile method to synthesize $PdH_{0.43}$ NCs with the shape of cube, octahedron and rhombic dodecahedron (RD), whose surface facets are {100}, {111} and {110}, respectively. The as-prepared $PdH_{0.43}$ NCs are highly stable and exhibit enhanced catalytic activity and extremely low overpotential towards electro-oxidation of formic acid compared with the commercial Pd black and three types of Pd NCs. The specific activity of the cubic $PdH_{0.43}$ NCs is more than five times that of the commercial Pd black and two times that of the cubic Pd NCs. Among the three types of $PdH_{0.43}$ NCs with different surface structure, the activity order is followed by $PdH_{0.43}$ {100} > $PdH_{0.43}$ {111} > $PdH_{0.43}$ {110}.**

Keywords: alloy, nanoparticles, palladium hydrides, surface structure, electrocatalytic activity

INTRODUCTION

The physical-chemical properties of noble metal based nanocrystals (NCs) are highly dependent on their size, composition and surface structure [1,2]. Controllable synthesis of noble metal based NCs with different surface structures is an important approach for achieving unique properties as well as enhanced performance in many important application fields [3,4]. Therefore, in the past decade, intensive studies have been carried out on controlling the noble NCs with various crystal facets exposed and exploring the relationship between exposed crystal facets and properties [5–7].

Pt-based electrocatalysts are commercially predominant for fuel cells, but they are high cost and in poor reserve [8,9]. As an alternative solution, Pd-based electrocatalysts have attracted much attention [10–12]. Palladium is also well-known for its high affinity with hydrogen, and it can adsorb large volumetric quantities of hydrogen at ambient condition to form PdH_x. Due to this unique property, Pd plays an important role in various fields of applications including hydrogen detection [13], hydrogen storage [14], hydrogen purification [15], catalysis for alkyne hydrogenation [16], and so on. On the other hand, when forming PdH_x by the adsorption of hydrogen, the electronic structure of Pd is modified, and thus its catalytic activity is also tuned compared with pure Pd catalysts. So far, the palladium hydrides are typically formed by direct exposure of the metal Pd to hydrogen gas at certain condition [17,18]. Besides, PdH_x can be also formed *via* a mild chemistry method by reacting Pd particle with aqueous borohydride [19] or by applying negative potential to drive the evolved hydrogen atoms into the lattice of Pd NCs [20]. However, these as-prepared PdH_x nanoparticles are usually unstable due to spontaneous releasing of hydrogen in ambient condition, and thus they are difficult to be good candidate as promising catalysts. To date, PdH_x nanoparticles were sparsely explored as the electrocatalyst for fuel cells, let alone PdH_x NCs with well refined surface structures.

Very recently, unexpected stable $PdH_{0.43}$ nanoparticles *via* a facile treatment of commercial Pd black with amines were successfully synthesized [21,22], exhibiting superior catalytic activity toward formic acid electro-oxidation

[1] State Key Laboratory for Physical Chemistry of Solid Surfaces, Collaborative Innovation Center of Chemistry for Energy Materials College of Chemistry and Chemical Engineering, Xiamen University, Xiamen 361005, China
[2] Pen-Tung Sah Institute of Micro-Nano Science and Technology, Xiamen University, Xiamen 361005, China
* Corresponding authors (emails: yqjiang@xmu.edu.cn (Jiang Y); zxxie@xmu.edu.cn (Xie Z))

[21]. To optimize the electrocatalytic performance of the stable $PdH_{0.43}$ nanoparticles, it is thus necessary to study the relevance between surface-structure and catalytic activity. In this paper, we report three types of $PdH_{0.43}$ NCs with different morphologies enclosed with {111}, {100} and {110} facets respectively by a two-step synthesis method. Compared with the pure Pd NCs and the commercial Pd black, the three as-prepared $PdH_{0.43}$ nanocatalysts served as highly efficient catalysts in the formic acid electro-oxidation reaction. They not only improve the maximum oxidation current density of the formic acid, but also greatly reduce the oxidation overpotential with the activity order as $PdH_{0.43}$ {100} > $PdH_{0.43}$ {111} > $PdH_{0.43}$ {110}.

EXPERIMENTAL SECTION

Chemicals and materials

Palladium(II) chloride ($PdCl_2$), sodium chloropalladite (Na_2PdCl_4), citric acid ($C_6H_8O_7$), polyvinylpyrrolidone (PVP, Mw=5500), L-ascorbic acid (AA), potassium iodide (KI), potassium bromide (KBr), sulfuric acid (H_2SO_4), formic acid (HCOOH) and ethanol (C_2H_5OH) were purchased from Sinopharm Chemical Reagent Co. Ltd. Commercial Pd black was purchased from Johnson Matthey. Hexadecyl trimethyl ammonium chloride (CTAC), hexadecyl trimethyl ammonium bromide (CTAB) and oleylamine ($C_{18}H_{37}N$) were purchased from J&K. *n*-Butylamine ($C_4H_{11}N$), *n*-hexylamine ($C_6H_{15}N$), ethanediamine ($C_2H_8N_2$), phenylamine (C_6H_7N), dodecylamine ($C_{12}H_{27}N$) and octadecylamine ($C_{18}H_{39}N$) were purchased from Alfa Aesar. Nitrogen (N_2, 99.99%) and mixed gas (4% CO + 96% N_2) were purchased from Linde Industrial Gases. All chemicals were used as received without further purification.

Preparation of $PdH_{0.43}$ NCs

$PdH_{0.43}$ NCs were prepared by a two-step method. Firstly, the cubic, octahedral and rhombic dodecahedral (RD) Pd NCs were synthesized *via* the modified method based on the references [23–25], respectively. Then, 2 mg of cubic/octahedral/RD Pd NCs was mixed with 10 mL of *n*-butylamine under magnetic stirring. The suspension was transferred to a Teflon-lined stainless-steel autoclave with a capacity of 25 mL. The sealed autoclave was heated from room temperature to 200°C in 60 min and kept at that temperature for 6 h, before it was naturally cooled to room temperature. The products were collected by centrifugation (9500 rpm for 5 min) and washed several times with ethanol.

Characterizations

The morphology and crystal structure of the as-prepared products were observed by scanning electron microscopy (SEM, Hitachi S4800) operating at acceleration voltage of 15 kV and high-resolution transmission electron microscopy (HRTEM, JEOL JEM 2100) with an acceleration voltage of 200 kV. The samples were prepared by dropping ethanol dispersion of samples onto carbon-coated copper TEM grids. The crystal phase of the as-prepared products was determined by the powder X-ray diffraction (XRD) pattern using a Rigaku Ultima IV X-ray diffractometer with Cu Kα radiation. The surface states and chemical compositions of products were analyzed by X-ray photoelectron spectroscope (XPS, K-Alpha+, Thermo fisher Scientific). All binding energies were calibrated using the contaminant carbon (C 1s = 284.8 eV).

Electrocatalytic measurement

Cyclic voltammograms (CV) were recorded using an electrochemical workstation (CHI 760e, Shanghai Chenhua Co., China). A glassy carbon electrode (diameter 5 mm) was carefully polished and washed before each experiment. The Pd or $PdH_{0.43}$ nanocatalysts were dispersed in ethanol and 5% nafion (volume ratio: 0.02%). The concentrations of the three catalysts were 1.0 mg mL^{-1}. In a typical experiment, 5 μL of the suspensions were deposited on the glassy carbon electrode as the working electrode. A carbon electrode and a saturated calomel electrode (SCE) were served as the counter electrode and the reference electrode, respectively. It should be noted that in order to remove possible organic adsorbates before other electrochemical measurement, the prepared Pd and $PdH_{0.43}$ catalysts were firstly electrochemically cleaned by continuous potential cycling between −0.25 and 0.90 V in 0.5 mol L^{-1} H_2SO_4 solution until a stable CV curve was obtained. For specific activity, the peak currents of nanocatalysts were all normalized to the electrochemically active surface area (ECSA). The ECSA was determined according to the equation ECSA = Q / q^0, where Q is the electric charge calculated from the area of the coulombic charge of the reduction of PdO at 25°C in N_2-saturated 0.5 mol L^{-1} H_2SO_4 solution, and q^0 is 430 μC cm^{-2} [26]. The catalytic activity was measured by CV in a solution containing 0.5 mol L^{-1} H_2SO_4 + 0.25 mol L^{-1} HCOOH at a scan rate of 50 mV s^{-1} from −0.25 to 0.80 V. For the CO stripping experiments in 0.5 mol L^{-1} H_2SO_4 solution, it was first purged with N_2 for 10 min, and then, the electrode was put into it, followed by CO purging for 15 min to allow the complete adsorption of CO onto the catalysts. After that, the electrode

was transferred to the electrochemical cell with 0.5 mol L^{-1} H_2SO_4 solution bubbled with N_2 for 10 min for CO stripping measurement. The CO stripping voltammogram was recorded from −0.25 to 0.80 V with a scan rate of 20 mV s^{-1}.

RESULTS AND DISCUSSION

The cubic, octahedral and RD $PdH_{0.43}$ NCs were prepared *via* a facial *n*-butylamine treatment of prefabricated Pd NCs. The TEM (Fig. 1a–c) and SEM images (Fig. S1) show that the shapes of the as-prepared $PdH_{0.43}$ NCs are well maintained from their precursors of Pd NCs (Figs S2, S3). The cubic, octahedral and RD $PdH_{0.43}$ NCs are enclosed by {100}, {111} and {110} facets, respectively. The Fourier transition images (Fig. 1g–i) based on HRTEM images of the single $PdH_{0.43}$ cubic, octahedral and RD NCs (Fig. 1d–f) confirm the nature of single crystallinity and the predominant surface facets of these nano-crystalline samples being {100}, {111} and {110} facets, respectively. The sizes of the three types of $PdH_{0.43}$ NCs are 21.1, 26.5 and 28.4 nm, respectively (Fig. S4). XRD patterns of the three synthesized $PdH_{0.43}$ NCs are shown in Fig. 2, the three patterns are similar, and all the diffraction peaks shift to low 2θ compared with Pd face centered cubic (fcc) structure with lattice parameter of 3.890 Å (JCPDS No. 46-1043). The negative shifts indicate the expansion of the Pd lattice, and the cell constant of the as-prepared three $PdH_{0.43}$ NCs is determined to be ca. 3.996(1) Å. It is about 2.7% larger than that of Pd NCs, suggesting incorporation of hydrogen in Pd lattice structure, that is, the successful formation of palladium hydrides in the synthetic condition. Based on the relationship between lattice parameter and composition within palladium hydride, the H/Pd ratio in the three types of as-prepared products is estimated to be 0.43, and thus the palladium hydrogen compounds are denoted as $PdH_{0.43}$. The H-content (0.43) in the three as-prepared palladium hydrides NCs with different surface structures is smaller than the minimum β-phase content (0.58) for the bulk samples, due to the nano-scaled effect [27].

XPS was conducted to study the chemical state and valence band structure of Pd element in $PdH_{0.43}$ NCs and the precursor Pd NCs. The high resolution XPS Pd 3d spectra show the presence of Pd ($3d_{3/2}$) and Pd ($3d_{5/2}$) peaks (Fig. 3a–c). The binding energy of these Pd NCs (335.25 eV) is very close to the value generally reported for metallic Pd in the literature [28], whereas the binding energy of Pd ($3d_{5/2}$) in $PdH_{0.43}$ NCs is 0.42 eV higher than that of Pd NCs, suggesting the adsorbate-induced surface core-level shift and the contribution from the formation of PdH_x. The valence band structures of the samples are

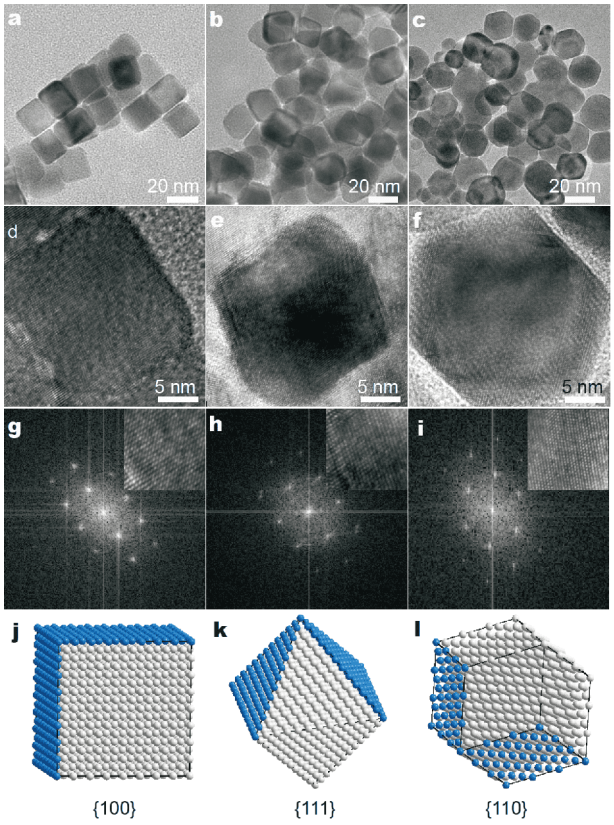

Figure 1 TEM and HRTEM images of $PdH_{0.43}$ NCs with (a, d) cubic, (b, e) octahedral and (c, f) RD shapes. (g–i) The corresponding Fourier transition images, the inset is the enlarged lattice fringes in (d–f). (j–l) The typical schematic models of cube, octahedron and RD of metallic fcc structures.

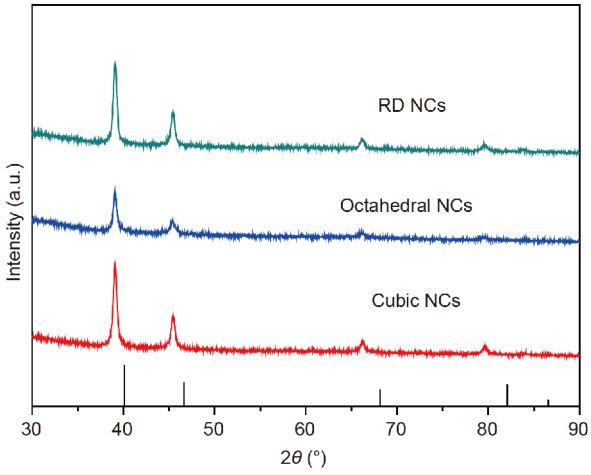

Figure 2 XRD patterns of $PdH_{0.43}$ with different morphologies. The black rod lines represent the standard Pd fcc structure (JCPDS No. 46-1043).

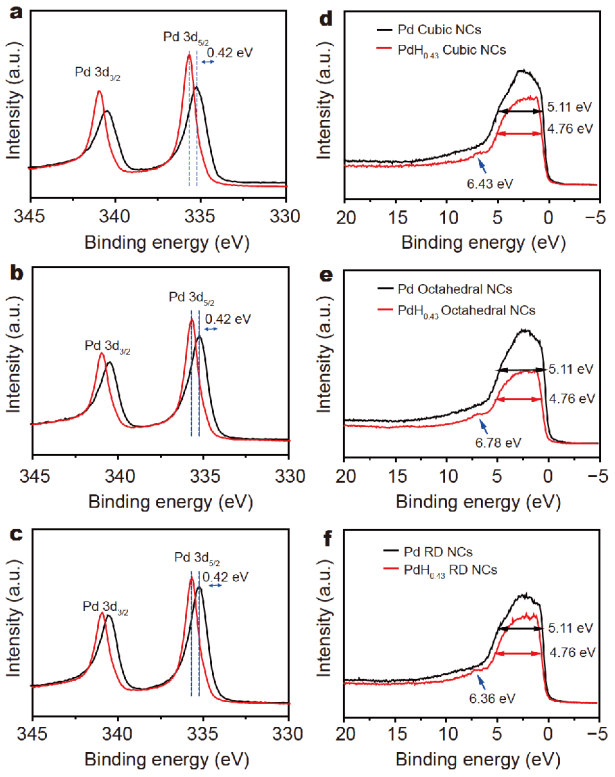

Figure 3 (a–c) XPS Pd 3d spectra and (d–f) XPS valence band structures of $PdH_{0.43}$ NCs (red curve) and Pd NCs (black curve) with different morphologies.

shown in Fig. 3d–f. Compared with Pd NCs, the full width at half maximum are reduced from ca. 5.11 eV in Pd NCs to 4.76 eV in $PdH_{0.43}$ NCs. The narrowed band width of 0.35 eV is caused by the larger Pd–Pd distance in the hydride [21]. At the same time, the small emission peaks were also observed at 6.43, 6.78 and 6.36 eV in the valence bands for cubic, octahedral and RD $PdH_{0.43}$ NCs, respectively, which may arise from the strong interaction between the Pd 4d and H 1s due to the formation of PdH_x [29]. All of these XPS evidences indicate that the precursor Pd NCs are completely converted to $PdH_{0.43}$ NCs, in good agreement with XRD analyses.

Our previous studies demonstrated the primary amine can release hydrogen along with the formation of corresponding secondary amine and imine in the presence of Pd catalyst [21]. We tried a series of amine to produce PdH_x NCs from Pd cubic NCs. Besides *n*-butylamine, *n*-hexylamine and ethanediamine can easily release hydrogen and lead to the formation of $PdH_{0.43}$ NCs, no PdH_x product was detected in the presence of octadecylamine and dodecylamine with relative longer alkyl chains (Fig. S5). Meanwhile, we got the mixture of Pd and $PdH_{0.43}$ NCs in the presence of oleylamine and phenylamine in this synthesis environment (Fig. S5). Therefore the selection of primary amine is crucial for the formation of high purity $PdH_{0.43}$ NCs. It is worth noting that when we tried *n*-butylamine treatment on three precursors of Pd NCs at ambient condition for three days, a subtle variation was observed. The shoulder peaks of Pd 3d in XPS spectra (Fig. S6a–c) are obviously different from the single peaks of Pd NCs or $PdH_{0.43}$ NCs in Fig. 3a–c. The shoulder peaks include adsorbate-induced surface core-level shift components, indicating distinct hydrogen incorporation. However, the XRD patterns (Fig. S6d) match well with that of standard Pd fcc structure, indicating H atoms are merely adsorbed on the surface of Pd NCs. We thus propose the formation of PdH_x NCs could divide into two steps, that is, the released H_2 is adsorbed on the surface of palladium at first, and then the dissociated hydrogen atoms intercalate into the crystal lattice of palladium.

We further conducted the time-dependent experiments in the formation of three types of $PdH_{0.43}$ NCs. From the time tracking XRD patterns (Fig. 4a–c), we found the cubic, octahedral and RD $PdH_{0.43}$ NCs ware thoroughly converted after 0.5, 4 and 6 h of reaction, respectively, indicating different forming rates for $PdH_{0.43}$ NCs with different morphologies. The forming rate of $PdH_{0.43}$ is consistent with the hydrogen absorption rate of Pd NCs, in which the order is Pd cube > Pd octahedron > Pd RD. Strikingly, those $PdH_{0.43}$ NCs are quite stable, their β-phase structure and H content of 0.43 are well preserved even after being kept at ambient condition for one year (their XRD patterns are shown in Fig. S7). The stability of three types of as-prepared $PdH_{0.43}$ NCs was further tested by annealing the samples in an argon atmosphere at 300°C for 2 h. As shown in Fig. 4d , after heat treatment, the cubic $PdH_{0.43}$ NCs maintain unchanged, RD $PdH_{0.43}$ NCs become Pd NCs thoroughly, while octahedral $PdH_{0.43}$ NCs turn out to be the mixture of Pd and PdH_x NCs. Among the three types of $PdH_{0.43}$ NCs, the heat stability obeys the order of $PdH_{0.43}$ {100} > $PdH_{0.43}$ {111} > $PdH_{0.43}$ {110}. The time-dependent and the heat-stability experiments reveal the difference regarding the hydrogen adsorption of Pd NCs and desorption of $PdH_{0.43}$ NCs with three low-index facets. A recent exploration also found two low-index facets ({100} and {111}) yielded significantly different desorption rates of hydrogen, where the desorption was thought to be governed by the surface-limited recombination of hydrogen atoms to form H_2 [30].

The successful syntheses of cubic, octahedral and RD

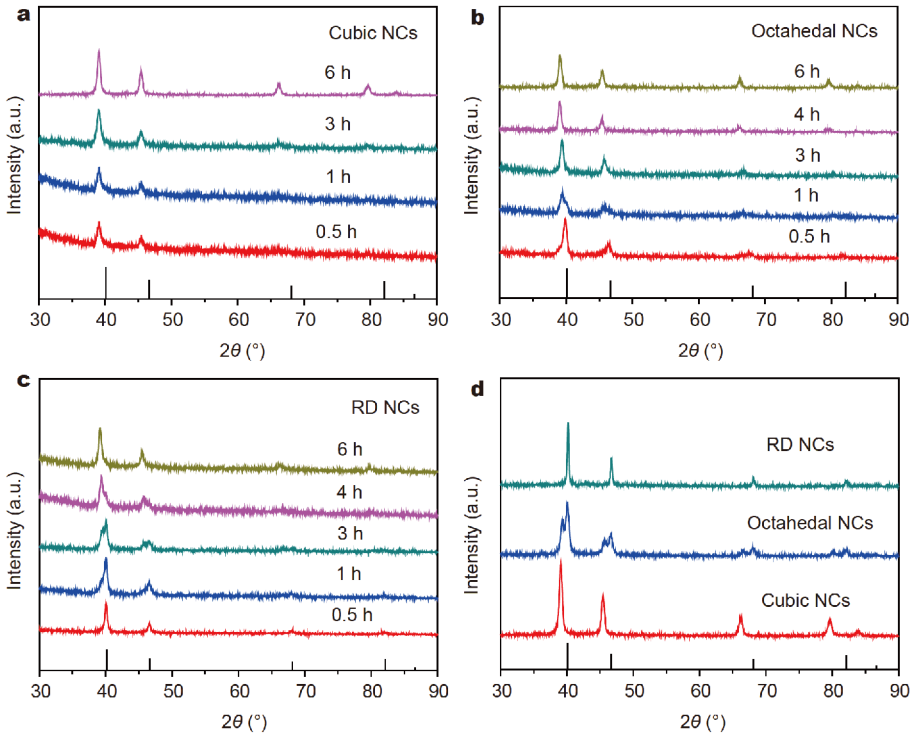

Figure 4 (a–c) Time tracking of XRD patterns during the synthesis of $PdH_{0.43}$ with reaction times of 0.5, 1, 3, 4 and 6 h. (d) XRD patterns of $PdH_{0.43}$ NCs after annealing under Ar atmosphere at 300°C for 2 h. The black rod lines represent the standard Pd fcc structure (JCPDS No. 46-1043).

$PdH_{0.43}$ NCs with similar size but different surface structures ({100}, {111} and {110}) provide us a good opportunity to study the structure-activity relationship among them. Here, we chose the formic acid electrooxidation reaction as a probe reaction, three untreated Pd NCs and commercial Pd black as the references. CV measurements were employed to examine the electrocatalytic activity of different catalysts. CV curves recorded in 0.5 mol L^{-1} H_2SO_4 solution exhibit distinct differences for $PdH_{0.43}$ and Pd NCs (Figs S8, S9). The peak currents of H desorption of the $PdH_{0.43}$ NCs are dozens of times higher than that of the Pd NCs, which can be attributed to the formation of β-phase PdH_x [20]. Fig. 5a–c show CV curves for $PdH_{0.43}$ and Pd NCs in 0.5 mol L^{-1} H_2SO_4 + 0.25 mol L^{-1} HCOOH solution (the specific catalytic activities and peak potentials of the catalysts are also summarized in Table S1). It can be found the peak current at positive scan on the cubic, octahedral and RD $PdH_{0.43}$ NCs is 11.1, 9.6, 7.8 mA cm^{-2}, while the value of Pd NCs with the same morphology is 5.2, 4.2 and 3.8 mA cm^{-2}, respectively. The peak current for commercial Pd black is 2.1 mA cm^{-2}. Thus, the specific activity of the cubic $PdH_{0.43}$ NCs is more than 5 times that of the commercial Pd black and more than 2 times that of the cubic Pd NCs. In fact, all three $PdH_{0.43}$ samples exhibit enhanced specific activity compared with Pd NCs and the Pd black, suggesting the enhanced catalytic performance towards formic acid oxidation of palladium hydride. It should be noted that the specific activity order of both $PdH_{0.43}$ and Pd NCs with three basal facets is followed by {100} > {111} > {100}. For a better comparison, we also compared the current density of different nanocatalysts at a fixed potential of 0.16 V (Table S1). Three $PdH_{0.43}$ nanocatalysts still exhibit the enhanced catalytic activity than those of the Pd nanocatalysts. Strikingly, besides the enhanced peak current density, the oxidation peak potentials of formic acid on the three types of $PdH_{0.43}$ NCs shift to much low potential. For instance, the peak potential of the cubic $PdH_{0.43}$ NCs is as low as 54 mV, which is much lower than that of the cubic Pd NCs (245 mV) and the commercial Pd black (316 mV), respectively. To largely decrease overpotential of formic acid oxidation reaction is a remarkable improvement for Pd-based NCs. Meanwhile, the peak potential for octahedral and RD $PdH_{0.43}$ are 61 and 63 mV, respectively. The similarity in decreasing peak potential on $PdH_{0.43}$ NCs with different basal facets implies it is the incorporation of hydrogen plays a vital role in affecting the oxidation potential sig-

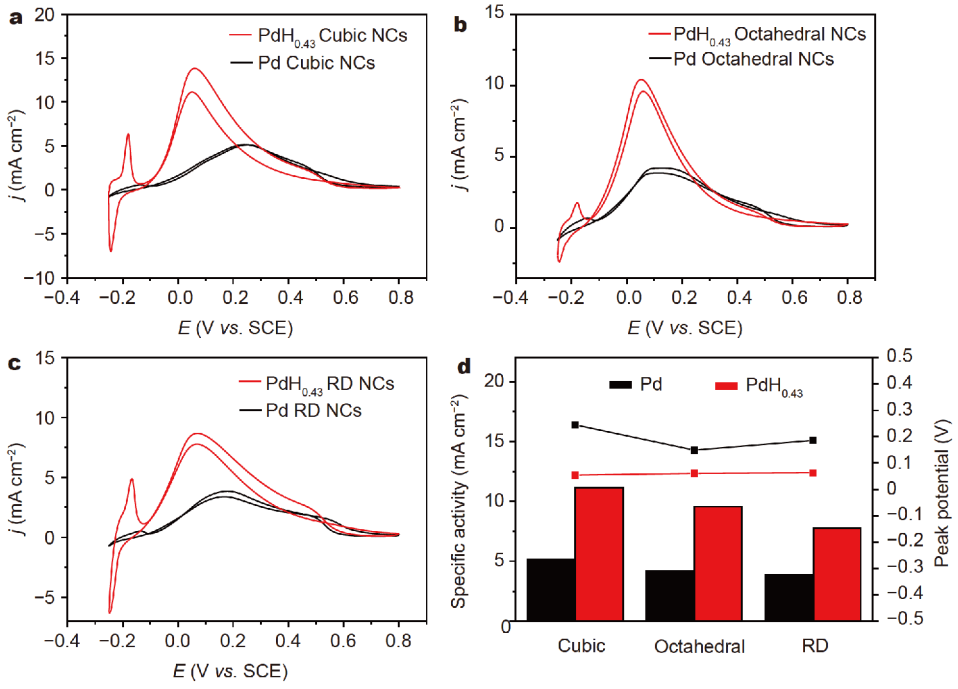

Figure 5 (a–c) CVs measured on $PdH_{0.43}$ and Pd NCs with different morphologies in 0.5 mol L^{-1} H_2SO_4 + 0.25 mol L^{-1} HCOOH (scan rate: 50 mV s^{-1}). (d) Comparison of specific activity (column) and peak potential (line) towards formic acid oxidation on $PdH_{0.43}$ and Pd NCs.

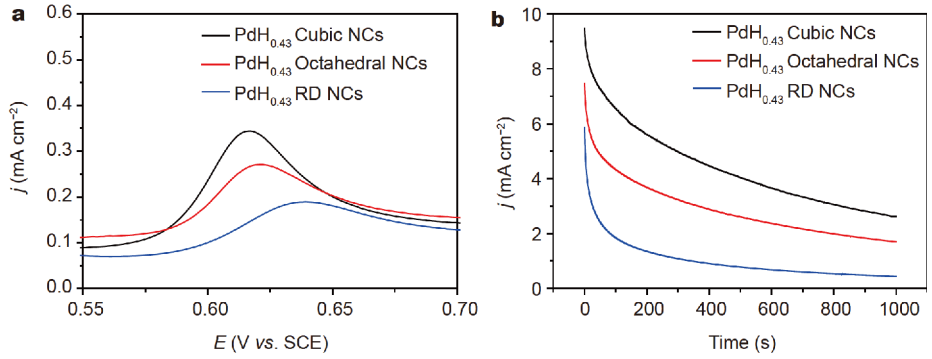

Figure 6 (a) CO-stripping curves in 0.5 mol L^{-1} H_2SO_4 (scan rate: 20 mV s^{-1}). (b) *i-t* curves for formic acid oxidation at 0 V (*vs.* SCE, at 298 K) on three $PdH_{0.43}$ NCs with different surface structures.

nificantly, but not the surface structure. Combining the experimental data and our previous studies, the enhanced catalytic performance could be attributed to the distinct electronic structure of PdH_x. The interaction of H with Pd would lead to the downshift of the Pd d-band center [21,31–35], which weakens the bonding interaction between noble metal atoms and reaction intermediates and thereby lows the onset oxidation potential. We further conducted CO electro-oxidation experiment to check the CO-tolerance property of the three as-prepared $PdH_{0.43}$ NCs (Fig. S10). As shown in Fig. 6a, The CO-stripping curves reveal the onset potentials of CO electro-oxidation on different $PdH_{0.43}$ NCs have a gradual upward trend with the order as cubic NCs < octahedral NCs < RD NCs. It means the $PdH_{0.43}$ NCs with {100} facets have the best CO-tolerance property among the three PdH_x NCs. In addition, the CO onset potential of $PdH_{0.43}$ NCs is lower than that of Pd NCs (Table S1), which proves their CO-tolerance property is improved. The catalytic durability of the three $PdH_{0.43}$ NCs was tested by chronoamperometric technique. The current-time (*i-t*) curves in Fig. 6b show cubic $PdH_{0.43}$ NCs keep the highest catalytic performance among the three NCs over the test. At the same time, the three $PdH_{0.43}$ NCs were collected and tested by powder

XRD after the electrochemical test (Fig. S11). By comparing the diffraction peaks of samples before and after electrochemical test, one can find that the phase structure and the composition of $PdH_{0.43}$ is unchanged, confirming good electrocatalytic stability of the three $PdH_{0.43}$ NCs toward the formic acid oxidation at working potential from −0.25 to 0.9 V.

CONCLUSIONS

In summary, we have successfully prepared three types of $PdH_{0.43}$ NCs with different morphologies, which are similar in size and enclosed with the facets of {100}, {111} and {110}, respectively. The electrochemical characterizations exhibit the enhanced catalytic performance when applying those $PdH_{0.43}$ NCs to the anode reaction of formic acid fuel cell compared with Pd NCs and commercial Pd black. The enhanced peak current density and negative shift of peak potential suggest that the as-prepared $PdH_{0.43}$ NCs have great potential in increasing both the current density and working voltage of fuel cells. Furthermore, the catalytic activity sequence for palladium hydride NCs with different surface structures follows the order of $PdH_{0.43}$ {100} > $PdH_{0.43}$ {111} > $PdH_{0.43}$ {110}. Most importantly, the present approach for the preparation of PdH_x with well-defined surface structure is facile and cost-effective, and therefore it is suitable for rational design of Pd-based nanocatalysts with promising performance.

Received 12 August 2019; accepted 18 September 2019; published online 25 October 2019

1 Xia Y, Xiong Y, Lim B, *et al.* Shape-controlled synthesis of metal nanocrystals: Simple chemistry meets complex physics? Angew Chem Int Ed, 2009, 48: 60–103
2 Yuan Q, Wang X. Aqueous-based route toward noble metal nanocrystals: Morphology-controlled synthesis and their applications. Nanoscale, 2010, 2: 2328–2335
3 Gan L, Cui C, Heggen M, *et al.* Element-specific anisotropic growth of shaped platinum alloy nanocrystals. Science, 2014, 346: 1502–1506
4 Zhou K, Li Y. Catalysis based on nanocrystals with well-defined facets. Angew Chem Int Ed, 2012, 51: 602–613
5 Chen Q, Yang Y, Cao Z, *et al.* Excavated cubic platinum-tin alloy nanocrystals constructed from ultrathin nanosheets with enhanced electrocatalytic activity. Angew Chem Int Ed, 2016, 55: 9021–9025
6 Li H, Fan Q, Ye J, *et al.* Excavated Rh nanobranches boost ethanol electro-oxidation. Mater Today Energy, 2019, 11: 120–127
7 Zhang J, Chen M, Chen J, *et al.* Synthesis of single-crystal hyperbranched rhodium nanoplates with remarkable catalytic properties. Sci China Mater, 2017, 60: 685–696
8 Fu QQ, Li HH, Ma SY, *et al.* A mixed-solvent route to unique PtAuCu ternary nanotubes templated from Cu nanowires as efficient dual electrocatalysts. Sci China Mater, 2016, 59: 112–121
9 Zhang L, Roling LT, Wang X, *et al.* Platinum-based nanocages with subnanometer-thick walls and well-defined, controllable facets. Science, 2015, 349: 412–416
10 Niu W, Zhang L, Xu G. Shape-controlled synthesis of single-crystalline palladium nanocrystals. ACS Nano, 2010, 4: 1987–1996
11 Chen A, Ostrom C. Palladium-based nanomaterials: Synthesis and electrochemical applications. Chem Rev, 2015, 115: 11999–12044
12 Duan L, Fu R, Xiao Z, *et al.* Activation of aryl chlorides in water under phase-transfer agent-free and ligand-free Suzuki coupling by heterogeneous palladium supported on hybrid mesoporous carbon. ACS Catal, 2014, 5: 575–586
13 Offermans P, Tong HD, van Rijn CJM, *et al.* Ultralow-power hydrogen sensing with single palladium nanowires. Appl Phys Lett, 2009, 94: 223110
14 Li G, Kobayashi H, Dekura S, *et al.* Shape-dependent hydrogen-storage properties in Pd nanocrystals: which does hydrogen prefer, octahedron (111) or cube (100)? J Am Chem Soc, 2014, 136: 10222–10225
15 Park ED, Lee D, Lee HC. Recent progress in selective CO removal in a H_2-rich stream. Catal Today, 2009, 139: 280–290
16 Teschner D, Borsodi J, Wootsch A, *et al.* The roles of subsurface carbon and hydrogen in palladium-catalyzed alkyne hydrogenation. Science, 2008, 320: 86–89
17 Kobayashi H, Yamauchi M, Kitagawa H, *et al.* On the nature of strong hydrogen atom trapping inside Pd nanoparticles. J Am Chem Soc, 2008, 130: 1828–1829
18 Oliveira MCF. A new approach to prepare highly loaded palladium. Electrochem Commun, 2006, 8: 647–652
19 Murphy DW, Zahurak SM, Vyas B, *et al.* A new route to metal hydrides. Chem Mater, 1993, 5: 767–769
20 Rose A, Maniguet S, Mathew RJ, *et al.* Hydride phase formation in carbon supported palladium nanoparticle electrodes investigated using *in situ* EXAFS and XRD. Phys Chem Chem Phys, 2003, 5: 3220
21 Zhang J, Chen M, Li H, *et al.* Stable palladium hydride as a superior anode electrocatalyst for direct formic acid fuel cells. Nano Energy, 2018, 44: 127–134
22 Zhao Z, Huang X, Li M, *et al.* Synthesis of stable shape-controlled catalytically active β-palladium hydride. J Am Chem Soc, 2015, 137: 15672–15675
23 Jin M, Liu H, Zhang H, *et al.* Synthesis of Pd nanocrystals enclosed by {100} facets and with sizes <10 nm for application in CO oxidation. Nano Res, 2011, 4: 83–91
24 Hong JW, Kim D, Lee YW, *et al.* Atomic-distribution-dependent electrocatalytic activity of Au-Pd bimetallic nanocrystals. Angew Chem Int Ed, 2011, 50: 8876–8880
25 Zhang HX, Wang H, Re YS, *et al.* Palladium nanocrystals bound by {110} or {100} facets: from one pot synthesis to electrochemistry. Chem Commun, 2012, 48: 8362–8364
26 Feng Y, Bin D, Yan B, *et al.* Porous bimetallic PdNi catalyst with high electrocatalytic activity for ethanol electrooxidation. J Colloid Interface Sci, 2017, 493: 190–197
27 Ingham B, Toney MF, Hendy SC, *et al.* Particle size effect of hydrogen-induced lattice expansion of palladium nanoclusters. Phys Rev B, 2008, 78: 245408
28 Brun M, Berthet A, Bertolini JC. XPS, AES and Auger parameter of Pd and PdO. J Electron Spectr Related Phenomena, 1999, 104: 55–60
29 Houari A, Matar SF, Eyert V. Electronic structure and crystal phase stability of palladium hydrides. J Appl Phys, 2014, 116: 173706

30 Johnson NJJ, Lam B, MacLeod BP, *et al.* Facets and vertices regulate hydrogen uptake and release in palladium nanocrystals. Nat Mater, 2019, 18: 454–458
31 Hammer B, Nielsen OH, Nrskov JK. Structure sensitivity in adsorption: CO interaction with stepped and reconstructed Pt surfaces. Catal Lett, 1997, 46: 31–35
32 Kitchin JR, Nørskov JK, Barteau MA, *et al.* Role of strain and ligand effects in the modification of the electronic and chemical properties of bimetallic surfaces. Phys Rev Lett, 2004, 93: 156801
33 Qi XQ, Wei ZD, Li L, *et al.* DFT study on interaction of hydrogen with Pd(111). Comput Theor Chem, 2012, 979: 96–101
34 Lu Y, Wang J, Peng Y, *et al.* Highly efficient and durable Pd hydride nanocubes embedded in 2D amorphous NiB nanosheets for oxygen reduction reaction. Adv Energy Mater, 2017, 7: 1700919
35 Zhu W, Kattel S, Jiao F, *et al.* Shape-controlled CO_2 electrochemical reduction on nanosized Pd hydride cubes and octahedra. Adv Energy Mater, 2019, 9: 1802840

Acknowledgements This work was supported by the National Natural Science Foundation of China (21771153, 21721001, and 21773190), and the Natural Science Foundation of Fujian Province (2018J01015).

Author contributions Xie Z and Jiang Y conceived the study and guided the whole project. Zhan C designed and performed the experiments. Li H and Li X participated in the materials preparation and data analysis; Jiang Y and Zhan C wrote the manuscript. All authors contributed to the general discussion.

Conflict of interest The authors declare no conflict of interest.

Supplementary information Experimental details and supporting data are available in the online version of the paper.

Chenyang Zhan received his BSc degree in applied chemistry from Hunan University in 2016. He is currently a master's graduate under the supervision of Assoc. Prof. Yaqi Jiang and Prof. Zhaoxiong Xie. His research focuses on the development of Pd-based nanocrystals with controllable morphology and their electrochemical catalytic properties.

Yaqi Jiang received her BSc degree (1986), MSc degree (1989) and PhD degree (2011) from the Department of Chemistry at Shanghai Jiao Tong University, Fuzhou University and Xiamen University, respectively. She has been an associate professor of physical chemistry at Xiamen University since 2004. Her current research interest mainly focuses on the structure-activity relationship of inorganic nanomaterials.

Zhaoxiong Xie received his BSc degree (1987), MSc degree (1990), and PhD degree (1995) in physical chemistry from Xiamen University, China. He worked as a postdoctoral fellow at the Centre d'Etudes de Saclay in France from 1997 to 1998. Since 2002, he has been a professor of physical chemistry at Xiamen University. His current research is focused on the surface/interface chemistry of inorganic nanomaterials.

不同表面结构$PdH_{0.43}$纳米晶的制备及其甲酸电氧化性能

詹晨阳[1], 李慧齐[1], 李学敏[1], 蒋亚琪[1*], 谢兆雄[1,2*]

摘要 制备具有确定形貌和表面结构的纳米晶为研究其构效关系提供了有效途径, 且有利于设计开发具有优异催化性能的纳米催化剂. 本研究发展了一种制备不同形貌$PdH_{0.43}$纳米晶的简易方法, 其形貌分别为立方体、八面体和菱形十二面体, 对应的裸露晶面分别为{100}, {111}和{110}晶面. 不同形貌$PdH_{0.43}$纳米晶都非常稳定. 其与商业Pd黑和三种纯Pd纳米晶相比, 在甲酸电催化氧化反应中显示出更高的催化活性和极低的氧化过电位. 立方体$PdH_{0.43}$纳米晶的催化活性分别高于商业Pd黑的5倍和立方体Pd纳米晶的2倍. 不同表面结构$PdH_{0.43}$纳米晶的催化活性依次为$PdH_{0.43}$ {100} > $PdH_{0.43}$ {111} > $PdH_{0.43}$ {110}.

